Published in Biomaterials.
Full reference: Yeoman MS, Reddy BD, Bowles HC, Bezuidenhout D, Zilla P, Franz T. A constitutive model for the warp-weft coupled non-linear behavior of knitted biomedical textiles. Biomaterials, 2010, 31(32), 8484-93

ORIGINAL ARTICLE

A Constitutive Model for the Warp-Weft Coupled Non-linear Behavior of Knitted Biomedical Textiles

M. S. Yeoman*

Continuum Blue Ltd., Tredomen Innovation and Technology Park, Hengoed, UK

B. D. Reddy

Centre for Research in Computational and Applied Mechanics, University of Cape Town, Rondebosch, South Africa

H. C. Bowles

Finite Element Analysis Services (Pty.) Ltd., Parklands, South Africa

D. Bezuidenhout, P. Zilla, T. Franz**

Cardiovascular Research Unit, Chris Barnard Department of Cardiothoracic Surgery, University of Cape Town, Observatory, South Africa

Abstract

Knitted textiles have been used in medical applications due to their high flexibility and low tendency to fray. Their mechanics have, however, received limited attention. A constitutive model for soft tissue using a strain energy function was extended, by including shear and increasing the number and order of coefficients, to represent the non-linear warp-weft coupled mechanics of coarse textile knits under uniaxial tension. The constitutive relationship was implemented in a commercial finite element package. The model and its implementation were verified and validated for uniaxial tension and simple shear using patch tests and physical test data of uniaxial tensile tests of four very different knitted fabric structures. A genetic algorithm with step-wise increase in resolution and linear reduction in range of the search space was developed for the optimization of the fabric model coefficients. The numerically predicted stress-strain curves exhibited non-linear stiffening characteristic for fabrics. For three fabrics, the predicted mechanics correlated well with physical data, at

least in one principal direction (warp or weft), and moderately in the other direction. The model exhibited limitations in approximating the linear elastic behavior of the fourth fabric. With proposals to address this limitation and to incorporate time-dependent changes in the fabric mechanics associated with tissue ingrowth, the constitutive model offers a tool for the design of tissue regenerative knit textile implants.
Keywords: Constitutive modelling, Finite element analysis, Mechanical properties, Surgical mesh, Tissue ingrowth

1. Introduction

Textile fabrics have been used in a variety of biomedical applications such as the augmentation and reconstruction of knee [1, 2] and shoulder [3, 4] ligaments and intervertebral disc replacement [5]. In the therapy of cardiovascular diseases, fabrics have been utilized for cardiac support devices [6, 7, 8], tissue regenerative vascular grafts [9] and prosthetic heart valves for percutaneous implantation [10]. The optimal design of such textile implants requires the knowledge and appropriate facilitation of the mechanical properties of the fabrics.

The study of fabric mechanics dates back to the work of Haas and Dietzius [11] on the development of airship fabrics. However, the first real model for fabric forces was presented by Peirce [12] who simplified the structure of a woven fabric as ideal rods. This work has led the way for theories on the geometrical and mechanical behavior of fabrics.

Much work has been done in forming mathematical relations for modeling the tensile deformation of fabrics. Kawabata et al. [13] looked at a linearization method in two zones to describe the tensile behavior of fabrics. Predicted stress-strain relationships based on strain energy principles were presented by Hearle and Shanahan [14] and more recently by King et al. [15], solving two systems of equations (geometric and mechanical) with physical yarn properties. Grosberg and associates presented a function which displayed an initially

*Principal corresponding author
**Corresponding author
Email addresses: mark@continuum-blue.com (M. S. Yeoman), thomas.franz@uct.ac.za (T. Franz)

high modulus [16, 17]. Alsawaf [18] characterized the tensile behavior of fabrics into two straight segments, one with an initially low modulus where decrimping occurred and another with a higher modulus representing yarn extension which occurred after a critical point.

Polynomial functions have also been used to describe nonlinear stress-strain tensile behavior of fabrics [19]. However, the use of high degree polynomials for function fitting has given rise to polynomial "wiggling" [20], where a number of maxima and minima are observed. Alternate functions have been proposed, such as exponential and logarithmic functions. Hu and Newton [21] established a number of exponential constitutive equations for woven fabrics under tension. These exponential expressions used one or two parameters to describe fabric behavior. The resulting solutions compared well with experimental data. However, only simple tensile tests were modeled, thus these models only represent a specific deformation state. They also use two separate sets of parameters for the warp and weft directions, and hence do not include coupling effects between the fabric warp and weft behavior. Since the early 1980s, advancement in this field has slowed due to the complex nature of the mathematical expressions needed to describe fabric behavior.

Bais-Singh and Goswami [22, 23] modeled the non-uniform deformation of spun-bound fabrics under uniaxial and biaxial tension. A bilinear relation similar to that proposed by Alsawaf [18] was utilized and showed good comparisons with experimental data. Orthotropic linear elastic [24, 25, 26, 27, 28, 29] and orthotropic hypoelastic material models [30, 31] were employed to analyze drape tests and forming processes of textiles. Yu et al. [32, 33] proposed a constitutive model representing separately the contribution of fiber directional properties and shear properties of the fabric. Numerical results correlated well with experimental data in some cases [24, 30] while predictions varied by 10% in other cases [25]. However, drape tests and fabric forming exhibit small strains and large deflection deformation which is not ideal for the large strain tensile deformation modes needed for knitted structures and medical implants. Due to the complexity of the problem these models have taken specific deformation modes into consideration and have ignored others.

Nadler et al. [34] presented a multiscale constitutive model combining the woven fabric as a continuum membrane at macroscale with a constitutive law for a pair of overlapping yarns

at microscale. A mesoscale approach was applied to model monofilament woven textiles [35, 36], using the Ramberg-Osgood isotropic nonlinear elastic constitutive model [37] for the fibers.

In this study, a new constitutive relation was proposed for knitted fabrics under uniaxial tensile behavior. A genetic algorithm (GA) was developed for the identification of values for the fabric material coefficients such that physical stress-strain relationships are described optimally for a variety of distinctly different anisotropic knit fabrics. The implementation of the constitutive model in a commercial finite element (FE) package (Abaqus®) was demonstrated through a user material subroutine (UMAT).

2. Materials and Methods

2.1. Structure of Knits

Knits are fabrics where yarns are inter-looped. Generally, knitted structures are not as stiff as their woven counterparts and are highly porous. Knitted fabrics encompass warp and weft knits. Warp knits, found in many medical implants, are complex compared to weft knits. Weft knit structures tend to be highly extendable but are structurally unstable, unless interlocking occurs. This interlocking tends to reduce extensibility but does help with elastic recovery. Advantages of knitted fabrics include that they are flexible and comfortable in nature, and they tend not to fray and unravel at the edges.

2.2. Formulation of the Fabric Material Model

Large strain formulations are required when describing coarse knit fabrics under tension. The fabric constitutive model assumed that the material is highly elastic and compressible. Viscoelastic effects were neglected and incompressibility was not enforced. Due to the small thickness compared to the in-plane dimensions of the fabric, plane stress was implemented under consideration of tension and shear deformation.

Since the non-linear stress-strain characteristics of fabrics are similar to those of soft tissue, it was proposed to adapt a strain energy function for soft tissue proposed by Chuong

and Fung [38]:

$$w(E) = \frac{C}{2} \exp\left(a_1 E_{\theta\theta}^2 + a_2 E_{zz}^2 + 2a_4 E_{\theta\theta} E_{zz}\right) . \tag{1}$$

By including shear and increasing the number and order of coefficients, the proposed fabric strain energy function in general two-dimensional form was obtained as

$$w(E) = \frac{C}{2} \exp x$$

$$\begin{aligned} x \;=\; & a_1 E_{11}^2 + a_2 E_{22}^2 + a_3\left(E_{12}^2 + E_{21}^2\right) + a_4\left(E_{11}E_{22}\right) + \\ & a_5 E_{11}^3 + a_6 E_{22}^3 + a_7\left(E_{12}^3 + E_{21}^3\right) + a_8\left(E_{11}^3 E_{22}\right) + a_9\left(E_{11}E_{22}^3\right) \end{aligned} \tag{2}$$

where C and a_i (i = 1 to 9) are fabric material coefficients.

An Abaqus® UMAT subroutine was utilized for implementation of the fabric constitutive model. The subroutine provided the material elasticity tensor, stress and solution dependent variable updates at each increment.

The discrete elasticity tensor is defined by

$$K_{ijkl}^{\sigma\varepsilon} = \frac{\partial \sigma_{ij}}{\partial \varepsilon_{kl}}, \tag{3}$$

where σ and ε are the stress and strain, respectively. For large strain computations an appropriate conjugate stress-strain measure is needed. Since the proposed strain energy function is already defined in terms of Green strain E an appropriate conjugate pair is Green strain and the second Piola-Kirchhoff stress S, which are defined as

$$E = \frac{1}{2}\left(\nabla u + (\nabla u)^T + (\nabla u)^T \nabla u\right) \tag{4}$$

and

$$S_{ij} = \frac{\partial w}{\partial E_{ij}} . \tag{5}$$

The stress was explicitly defined as Cauchy 'true' stress using the relationship between Cauchy stress and second Piola-Kirchhoff stress in the form

$$\sigma_{ij} = J^{-1} F_{ik} S_{kl} F_{jl} . \tag{6}$$

Unlike the model by Chuong and Fung [38], Eq. (1), incompressibility was not enforced. For the implementation in Abaqus®, the following special operators were used. *Orientation*: defined the transverse fabric directions to ensure the material properties remained orientated as elements rotated and deformed; *Membrane element thickness*: A thickness of 100 μm was assigned to the membrane elements that were used to model the fabric; *Poisson's ratios* υ_{13} *and* υ_{31}: The use of membrane elements ensured a state of plane stress, thus the thickness was assumed to be constant.

2.3. Assessment of Constitutive Model Coefficients

Single and multiple element patch tests were utilized to assess the influence of the material coefficients (C, a_1, a_2, a_3, a_4, a_5, a_6, a_7, a_8 and a_9) and the effects of element orientation and type under uniaxial tensile and simple shear deformation. The single element models used a four-noded bilinear membrane element with boundary and load conditions describing the two modes of deformation, as illustrated in Fig. 1(a) and (b). Arbitrary fabric coefficients were employed and varied slightly to observe their influence on stress and strain behavior. The effect of element type and orientation was assessed, in tension and shear, with a uniform mesh with consistently ordered four-noded membrane elements and a non-uniform mesh with three and four-noded membrane elements, Fig. 1(c) and (d).

2.4. Experimental Characterization of Fabric Samples

To assess the ability of the constitutive model to simulate the physical fabric mechanics, four distinctly different fabrics were obtained (Finitex (Pvt.) Ltd., Cape Town, South Africa): 1) basic warp knit, 2) warp knit with Lycra® support, 3) coarse warp knit and 4) monofilament warp knit. The selected fabrics were part of standard production lots that underwent routine quality assessment with regard to consistency. Figure 2 provides scanning electron micrographs of the fabrics. Uniaxial tensile tests were performed on samples with dimensions 60 × 20 mm at 37 °C (Instron® 5544, Instron Corp., Norwood, MA), see Fig. 3a. The loading protocol comprised: 1) Pre-load to 1 % nominal strain at a strain rate of 50 mm/min to reduce material inconsistencies, and 2) Extension to 50 % nominal

strain at a strain rate of 200 mm/min, the strain rate stipulated by medical implant authorities [39, 40, 9]. Due to difficulties in monitoring lateral strain effects during the Instron® tests, caused by curling effects at the sample edges, fabric samples were strained on a flat bed at 37 °C in steps of 10, 20 and 30 %. For both the Instron® and the flat bed tests, a 5×5 mm grid was marked on each sample to visualize localized strain effects. Strengthening stitches were sewn at both ends of the samples to minimize localized stress concentrations. Using digital images recorded during the tests, the longitudinal and transverse strain was determined from a single grid cell located in the center of the sample.

2.5. Implementation and Validation of the Fabric Constitutive Equation

A quarter-symmetric FE model was used to simulate the physical uniaxial tensile tests. The model, see Fig. 3b, utilized a mesh of four-noded membrane elements. The boundary conditions were selected such that edge AB was free to move horizontally but constrained vertically, while edges AD and DC were free to move vertically but constrained horizontally. A quasi-static displacement at 200 mm/min [39, 40] was applied to edge DC. The loaded boundary DC and the edge BC were expected to have a greater variation in stress and deformation. Hence the element mesh was refined toward these edges. The mesh sensitivity was assessed by increasing and biasing the element density toward edges BC and DC and center point A until the stress, strain and displacement fields became consistent.

A genetic algorithm (GA), programmed using Perl®, is utilized to iteratively optimize the fabric model coefficients to represent the physically tested fabrics. Using a single set of fabric coefficients, the GA runs mutually orthogonal uniaxial tensile FE models in order to predict stress-strain curves for the warp and weft directions. Subsequently, the GA analyzes the predicted results with respect to the fit with physical test data utilizing objective, penalty and fitness functions. This process is repeated until a desired fitness value $f(C, a_i)$ is achieved or when 50 generations have been reached.

2.5.1. Dynamic Range and Resolution of the Search Space

The search space of the GA is dynamically confined and refined over the generations. An initial large range with low resolution allows the GA to maximize its initial search over a

wide search space. With increasing generations, the range of the search space is reduced and the resolution is increased, in order to constrain the GA for the refinement of the acceptable solutions obtained. Using initial values of $C = 10000$ and $a_i = 10$ (i = 1 to 9), the initial search ranges, $\{R\}$, of $0 < C \leqslant 20000$ and $0 \leqslant a_i \leqslant 20$ (i = 1 to 9) are biased $3:2$ between the first and second ranked solutions of the previous generation. In addition, the search space range is reduced linearly by 2.5 % over each generation. An explicit constraint for the search space range of C ensures that its value remains positive over the generations, $C|C \geq 0$, to prevent unrealistic compressive or zero stress solutions under tensile strain of the fabric.

The resolution of the search space is increased after each generation. A binary number of m bit is used to encode each scaled coefficient into the chromosome. With the initial value of $m = 5$, the resolution of the search space, $\{R\}/2^m$, is $20/2^5 = 0.625$ for a_i and $20000/2^5 = 625$ for C. The bit size is increased by 1 every 10^{th} generation, reaching $m = 10$ at the 50^{th} generation. Consequently, the range $\{R\}$ is reduced by 50%, the final resolution is $10/2^{10} = 9.7656 \times 10^{-3}$ for a_i and $10000/2^{10} = 9.7656$ for C. Figure 4 illustrates the reduction of the range and increase of resolution a two-dimensional parameter search space.

2.5.2. Objective, Penalty and Fitness Functions

The same set of fabric material model coefficients are utilized in two FE models that describe uniaxial tension in the warp and weft direction, respectively. This is implemented in the FE model by swapping the material model coefficients a_1 with a_2, a_5 with a_6, and a_8 with a_9. For the warp and weft directions, the numerical results for axial stress ($\sigma_{A,i}^{Model}$), localized axial strain ($\varepsilon_{A,i}^{Model}$), and localized transverse strain ($\varepsilon_{T,i}^{Model}$) are compared with the equivalent physical data of axial stress ($\sigma_{A,i}^{Data}$), localized axial strain ($\varepsilon_{A,i}^{Data}$) and localized transverse strain ($\varepsilon_{T,i}^{Data}$) at pre-defined axial strains of 10, 20 and 30 %.

Partial Objective Functions. The partial objective functions are calculated from the normalized differences between the model and physical data, illustrated in Fig. 5 for a single

orientation of one fabric. The partial objective functions for stress are

$$\phi^{\sigma_A^n} = \frac{\sum_{i=10\%,10\%}^{30\%} w_{\sigma_{A,i}}^n \left[1 - \left\{\left|\triangle\sigma_{A,i}^n\right| \left(\frac{1}{m_{\sigma_{A,i}}^n - 1}\right)\right\}\right]}{\sum_{i=10\%,10\%}^{30\%} w_{\sigma_{A,i}}^n}, \tag{7}$$

with

$$\triangle\sigma_{A,i}^n = \frac{\sigma_{A,i}^{Model,n} - \sigma_{A,i}^{Data,n}}{\sigma_{A,i}^{Data,n}}, \tag{8}$$

and

$$m_{\sigma_{A,i}}^n = \left\{\begin{array}{l} 1 + \left|\frac{\sigma_{A,i}^{\max,n} - \sigma_{A,i}^{Data,n}}{\sigma_{A,i}^{Data,n}}\right| \text{ for } \sigma_{A,i}^{Model,n} > \sigma_{A,i}^{Data,n} \\ 1 + \left|\frac{\sigma_{A,i}^{\min,n} - \sigma_{A,i}^{Data,n}}{\sigma_{A,i}^{Data,n}}\right| \text{ for } \sigma_{A,i}^{Model,n} \leq \sigma_{A,i}^{Data,n} \end{array}\right\}. \tag{9}$$

where n is the direction of the uniaxial tensile test (warp or weft), i the pre-defined axial strains of 10, 20 and 30%, $w_{\sigma_A}^n$ are the weightings for the pre-defined axial strain field values,

Similarly, the partial objective functions for localized axial strains are

$$\phi^{\varepsilon_A^n} = \frac{\sum_{i=10\%,10\%}^{30\%} w_{\varepsilon_{A,i}}^n \left[1 - \left\{\left|\triangle\varepsilon_{A,i}^n\right| \left(\frac{1}{m_{\varepsilon_{A,i}}^n - 1}\right)\right\}\right]}{\sum_{i=10\%,10\%}^{30\%} w_{\varepsilon_{A,i}}^n} \tag{10}$$

where

$$\triangle\varepsilon_{A,i}^n = \frac{\varepsilon_{A,i}^{Model,n} - \varepsilon_{A,i}^{Data,n}}{\varepsilon_{A,i}^{Data,n}}, \tag{11}$$

$$m_{\varepsilon_{A,i}}^n = \left\{\begin{array}{l} 1 + \left|\frac{\varepsilon_{A,i}^{\max,n} - \varepsilon_{A,i}^{Data,n}}{\varepsilon_{A,i}^{Data,n}}\right| \text{for } \varepsilon_{A,i}^{Model,n} > \varepsilon_{A,i}^{Data,n} \\ 1 + \left|\frac{\varepsilon_{A,i}^{\min\, n} - \varepsilon_{A,i}^{Data,n}}{\varepsilon_{A,i}^{Data,n}}\right| \text{ for } \varepsilon_{A,i}^{Model,n} \leq \varepsilon_{A,i}^{Data,n} \end{array}\right\}. \tag{12}$$

The partial objective functions for local transverse strains are

$$\phi^{\varepsilon_T^n} = \frac{\sum_{i=10\%,10\%}^{30\%} w_{\varepsilon_{T,i}}^n \left[1 - \left\{\left|\triangle\varepsilon_{T,i}^n\right| \left(\frac{1}{m_{\varepsilon_{T,i}}^n - 1}\right)\right\}\right]}{\sum_{i=10\%,10\%}^{30\%} w_{\varepsilon_{T,i}}^n}, \tag{13}$$

where

$$\triangle\varepsilon_{T,i}^{n} = \frac{\varepsilon_{T,i}^{Model,n} - \varepsilon_{T,i}^{Data,n}}{\varepsilon_{T,i}^{Data,n}} \ , \tag{14}$$

$$m_{\varepsilon_{T,i}}^{n} = \left\{ \begin{matrix} 1 + \left| \frac{\varepsilon_{T,i}^{\max,n} - \varepsilon_{T,i}^{Data,n}}{\varepsilon_{T,i}^{Data,n}} \right| & \text{for } \varepsilon_{T,i}^{Model,n} > \varepsilon_{T,i}^{Data,n} \\ 1 + \left| \frac{\varepsilon_{T,i}^{\min,n} - \varepsilon_{T,i}^{Data,n}}{\varepsilon_{T,i}^{Data,n}} \right| & \text{for } \varepsilon_{T,i}^{Model,n} \leq \varepsilon_{T,i}^{Data,n} \end{matrix} \right\} . \tag{15}$$

The differences $\triangle\sigma_{A,i}^{n}$, $\triangle\varepsilon_{A,i}^{n}$ and $\triangle\varepsilon_{T,i}^{n}$ are normalized and weighted to ensure that those solutions which model the test results accurately at lower strains are retained for further generations. The partial objective values tend to unity as model stresses, localized axial and transverse strains tend toward physical data. Similarly, parameters $m_{\sigma_{Ai}}^{n}$, $m_{\varepsilon_{Ai}}^{n}$ and $m_{\varepsilon_{Ti}}^{n}$ are multiples used to bias future generations from a certain side and partially penalize their respective partial objective functions.

Partial Penalty Functions. The partial penalties and weightings for the GA are as follows:

$$\text{if } \left\{ \sigma_{A,i}^{n} | \sigma_{A,i} \leq \sigma_{A,i}^{\min,n} \text{ and } \sigma_{A,i} \geq \sigma_{A,i}^{\max,n} \right\} \text{ then } \phi^{\sigma_A^n} \text{ are negatively weighted ;} \tag{16}$$

$$\text{if } \left\{ \varepsilon_{A,i}^{n} | \varepsilon_{A,i}^{n} \leq \varepsilon_{A,i}^{\min,n} \text{ and } \varepsilon_{A,i}^{n} \geq \varepsilon_{A,i}^{\max,n} \right\} \text{ then } \phi^{\varepsilon_A^n} \text{ are negatively weighted ;} \tag{17}$$

$$\text{if } \left\{ \varepsilon_{T,i}^{n} | \varepsilon_{T,i}^{n} \leq \varepsilon_{T,i}^{\min,n} \text{ and } \varepsilon_{T,i}^{n} \geq \varepsilon_{T,i}^{\max,n} \right\} \text{ then } \phi^{\varepsilon_T^n} \text{ are negatively weighted ;} \tag{18}$$

$$w_{x,10\%}^{n} > w_{x,20\%}^{n} > w_{x,30\%}^{n}. \tag{19}$$

In Eq. (19), x represents either axial stress σ_A, localized axial strain ε_A, or localized transverse strain ε_T. This ensures that numerical models which do not run to completion are weighted accordingly. Tests which fail to reach 10 % axial strain are given a lower ranking to those which reach an axial strain of 20 %, similarly for 20 and 30 %, thus favoring those models which run to completion.

Objective Function. The objective function is represented in terms of the partial objective functions by

$$\phi = \frac{w_{obj}^{\sigma_A^{Warp}} \phi^{\sigma_A^{Warp}} + w_{obj}^{\sigma_A^{Weft}} \phi^{\sigma_A^{Weft}} + w_{obj}^{\varepsilon_A^{Warp}} \phi^{\varepsilon_A^{Warp}} + w_{obj}^{\varepsilon_A^{Weft}} \phi^{\varepsilon_A^{Weft}} + w_{obj}^{\varepsilon_T^{Warp}} \phi^{\varepsilon_T^{Warp}} + w_{obj}^{\varepsilon_T^{Weft}} \phi^{\varepsilon_T^{Weft}}}{w_{obj}^{\sigma_A^{Warp}} + w_{obj}^{\sigma_A^{Weft}} + w_{obj}^{\varepsilon_A^{Warp}} + w_{obj}^{\varepsilon_A^{Weft}} + w_{obj}^{\varepsilon_T^{Warp}} + w_{obj}^{\varepsilon_T^{Weft}}} \ , \tag{20}$$

where w^i_{obj} are pre-defined weightings and i represents the partial objective function to which the weightings apply. These weightings are used to bias the objective value to either the warp or weft direction, to stresses, to localized axial and or transverse strains. From Eq. (20), ϕ will tend to unity as $\phi^{\sigma_A^{Warp}}$, $\phi^{\sigma_A^{Weft}}$, $\phi^{\varepsilon_A^{Warp}}$, $\phi^{\varepsilon_A^{Weft}}$, $\phi^{\varepsilon_T^{Warp}}$ and $\phi^{\varepsilon_T^{Weft}}$ tend to unity.

Global Penalty Functions. The penalty functions, p, are defined as

$$\text{if } \sigma^n_{A,10\%} \leqslant 0.0 \text{ then } p = -\infty \text{ else } p = 1 \ , \tag{21}$$

$$\text{if } \sigma^n_{T,10\%} \leqslant 0.0 \text{ then } p = -\infty \text{ else } p = 1 \ , \tag{22}$$

$$\text{if } \varepsilon^n_{T,10\%} \geqslant 0.0 \text{ then } p = -\infty \text{ else } p = 1 \ , \tag{23}$$

and ensure that the models run and the results obtained are reasonable and acceptable.

Fitness Function. The fitness function, f, for the GA for the comparison of model solutions and physical data for warp and weft uniaxial tension is:

$$f = p \times \phi \ . \tag{24}$$

3. Results

3.1. Assessment of Constitutive Model Coefficient and Verification of Constitutive Relationship

3.1.1. Single Element Models

Figure 6 displays the stress-strain curves and the normalized stress, obtained from dividing the stress values obtained at 20% tensile strain and 10% shear strain by the stress values achieved with that of the model with $C = 10000$ and $a_i = 10$. The numerically predicted stress-strain curves (Fig. 6a) exhibit a nonlinear stiffening effect characteristic for fabrics. Defining the subscripts i and j to denote the direction of uniaxial tension and the transverse direction, respectively, the following was observed (Note: The results in Fig. 6 are for $i = 2$ being the direction of uniaxial tension). As expected, the magnitude of stress increased proportionately with C. The *nonlinear stiffening effect*: greatly increased with increasing coefficients that affect terms containing E^2_{ii}, i.e. a_1 and a_2; moderately increased

with increasing coefficients that affect terms E_{ii}^3, i.e. a_6; slightly increased with increasing coefficients that affect $E_{jj}^3 E_{ii}$, i.e. a_8; greatly decreased with increasing coefficients affecting $E_{ii}E_{jj}$, i.e. a_4; slightly decreased with increasing coefficients that affect E_{jj}^3 and $E_{jj}E_{ii}^3$, i.e. a_5 and a_9; and was not affected by changing coefficients that affect E_{ij}, i.e. a_3 and a_7. The effect of changing a_1 through a_9 depended on the power of the strain terms to which they contribute. Those that affect lower order terms had a larger influence, as expected.

Further information was gained from the normalized stress and the associated transverse strain (Fig. 6b). The magnitude of axial and transverse stress was proportional to C; however, transverse strain was not affected by C. The *transverse strain, or Poisson's effect*: increased with increasing coefficients that affect product terms $E_{jj}E_{ii}$ and $E_{jj}E_{ii}^3$, i.e. a_4 and a_9; decreased with increasing coefficients that affect E_{jj}^2, E_{jj}^3 and $E_{jj}^3 E_{ii}$, i.e. a_1, a_5 and a_8; and was not affected by a_2, a_3, a_6 and a_7. The *axial and transverse stress*: both increased with increasing coefficients that a_2 and a_6 that affect terms E_{ii}^2 and E_{ii}^3, with axial stress being dominant; both decreased with increasing a_4, a_5, a_8 and a_9, with a predominant change in transverse stress for the latter two; and increased and decreased, respectively, with increasing coefficients that affect E_{jj}^2, i.e. a_1.

Negative coefficients a_i typically reduced transverse strain. A negative a_4 produced a negative normalized transverse strain, indicating positive strains in this direction. Negative a_2 and a_6 reduced the stress values but did not affect the transverse strain. Negative a_4 and a_9 increased the axial stress while reducing the transverse stress. Negative a_5 did not change the axial stress but reduced the transverse stress. Negative a_2 and a_6 caused compressive axial stress whilst in tension, which is unrealistic. Negative a_8 reduced both the axial and transverse stress values considerably. Negative a_7 did not affect the stress and transverse strain. (Note: the FE models did not converge upon a solution for negative a_1 and a_3.)

Figure 6(c) shows typical curves of shear stress versus shear angle obtained from the simple shear model. Although not clearly observed, the shear stress-strain relation became slightly curved by increasing coefficients a_3 and a_7.

3.1.2. Multi-element Fabric Meshes

Table 1 summarizes the results of the comparative tests with the uniform and non-uniform multi-element models and the single element model for uniaxial tensile and simple shear. Figure 7 illustrates the corresponding stress fields of the shear test models. No differences were observed between the two multi element models, and the single element model.

3.2. Implementation and Validation of the Fabric Constitutive Model

For the four fabric samples, convergence of the GA on a set of single solutions was found after 47, 42, 39 and 45 generations, respectively. Table 2 provides the model coefficients and the fitness, objective and partial objective values obtained from the GA for each fabric. The fitness values coincide with the objective values, all of which closely approach unity. The average partial objective values obtained for fabrics 1 to 4 are 0.99976 ± 0.00020, 0.99971 ± 0.00021, 0.99973 ± 0.00026 and 0.99968 ± 0.00027, respectively.

Figure 8 compares model predictions, obtained using the coefficients identified with the genetic algorithm, see Table 2, for the axial nominal stress versus axial engineering strain (Fig. 8 A-D) and transverse engineering strain versus axial engineering strain (Fig. 8 E-H) with data obtained from physical tests.

For experimental axial stress and axial strain, fabric samples 1, 3 and 4 exhibited a high degree of anisotropy and nonlinear stress-strain relationships in both the warp and weft directions, see Fig. 8 A, C, D. For these three fabrics, the model solutions fit excellently to test data in either the warp direction (fabric 1) or the weft direction (fabrics 3 and 4), while a reasonable fit between model and test data is obtained in the respective transverse direction. For fabric 2, the physical test data indicated a nearly linear stress-strain relationship in the weft direction and a lower degree of anisotropy (Fig. 8 B). Considerable deviation was observed between the model and physical data for this fabric.

For transverse strain versus axial strain, fabric 1 exhibited a difference between model and test data of $< 1.2\,\%$ in weft direction and $< 20\,\%$ in warp direction (Fig. 8 E). Close correlation between model and test was obtained for fabric 2 (Fig. 8 F), with differences

of $< 1\,\%$ and $1.5\,\%$ in the warp and weft direction, respectively. However, the solution for fabric 2 was largely linear, while fabric 1 showed an increase in Poisson's effect with an increase in axial strain. Large differences were observed for fabric 3 (Fig. 8 G) and fabric 4 (Fig. 8 H), except for the weft direction for fabric 3 with a small difference between model and test data of $< 2\,\%$ in transverse strain.

4. Discussion

The anisotropic nonlinear elastic constitutive model proved feasible to describe the nonlinear mechanics of a variety of fabrics under tensile loading and a linear characteristic under shear. These characteristics depended heavily on the fabric model coefficients used to describe the material properties. The exponential strain energy model does, however, not include anisotropic viscoelastic and plastic components, which are complex to model and implement [41], and fall outside the scope of this study.

It was found from the fabric patch tests that C, a_1, a_2, a_3 and a_4 should remain positive to ensure realistic fabric uniaxial tensile solutions. Negative coefficients would produce unrealistic compressive stresses. It is apparent from Eq. (3) that the magnitude and ratio of the coefficients contribute to the change in stress and strain. Thus, observations were only made for specific changes in the magnitude of the coefficients, namely, $1.5\times$ and $-1\times$. The predicted stress distributions were equal and uniform throughout the elements for the various patch test models employed, indicating that the material model was implemented correctly in the FE package. The stress-strain curves for simple shear exhibited a linear relationship, with nearly constant elastic modulus. While this is uncharacteristic for fabrics which typically feature a high initial modulus that decreases with increasing shear strain [42]. However, the latter was reported for a shear angle of between $0 - 0.8^\circ$ only, after which the relation became predominantly linear which agreed with the predicted solutions presented here.

The fabric model was validated against uniaxial tensile test data for four very different fabrics. The principal advantages of the GA developed for the optimization of the fabric model coefficients was the dynamic search space since the final coefficient values diverged

considerably from the initial starting values of $C = 20000$ and $a_i = 20$ (see Table 2). The step-wise increase in the resolution of the search space was implemented to search a coarse grid over N generations before being refined. With the linear reduction of the range of the search space after each generation, it was found that the step-wise increase of the resolution after N generations was not necessarily effective, as this limited the widespread searching capabilities of the GA. The implementation and magnitude of these GA features can easily be adjusted. Thus, weightings for the partial objective functions can be adjusted accordingly, allowing the GA to optimize on certain criteria first or in a biased fashion.

Good correlations were observed for three fabrics (1, 3 and 4) with typically one of the two directions, warp or weft, exhibiting a superior fit between model and physical data over the other direction (Fig. 8). For the fourth fabric (2) which showed a linear stress-strain relation in the weft direction, convergence on coefficients to properly describe the fabric was however not realized.

Variation between the optimized numerical solutions and the physical data may have different causes:

1. The strain-energy function used to describe the fabrics behavior does not allow for both linear and nonlinear stress-strain relations.
2. The fitness function was ineffective allowing the GA to converge on a suboptimal solution.
3. The penalty function and constraints caused potential generations to be lost if they slightly violated the constraints.

The fitness function utilized a normalized difference method with weighting to give a higher ranking to those generation members that modeled the lower strains better. Since good solutions were obtained for fabric samples 1, 3 and 4, the objective and fitness functions are assumed to be functional. The same applies to the penalty functions and constraint criteria that were sufficient to find good solutions for these three fabrics. The number of generations lost due to the penalty functions and constraints was not different for fabric 2 compared to fabrics 1, 3 and 4. Thus, it is seen to be the fabric constitutive model which is

causing the GA's inability to converge upon reasonable solutions for the linear stress-strain fabric relation.

To possibly overcome this limitation, a combined polynomial and exponential function could be used, e.g. as proposed by Tong and Fung [43]:

$$W = P + \frac{C}{2}\, e^{Q},$$

$$P = \frac{1}{2}\ \left[\alpha_1 E_{11}^2 + \alpha_2 E_{22}^2 + \alpha_3 \left(E_{12}^2 + E_{21}^2\right) + \alpha_4 E_{11} E_{22}\right], \tag{25}$$

$$Q = a_1 E_{11}^2 + a_2 E_{22}^2 + a_3 \left(E_{12}^2 + E_{21}^2\right) + a_4 E_{11} E_{22} + \gamma_1 E_{11}^3 + \gamma_2 E_{22}^3 + +\gamma_3 E_{11}^2 E_{22} + \gamma_5 E_{11} E_{22}^2.$$

This strain energy function was shown to give greater anisotropy and variation in the transverse directions. A similar function could be utilized to cater for the linear stress-strain components. These were not captured satisfactorily with the current model which was observed for fabric 2 that exhibited a linear stress-strain relationship. However, 13 coefficients would need to be solved for when using this function, and the term P in Eq. (25) may cause "polynomial wiggling", giving unrealistic fabric behavior [44].

Other alternatives may be discrete models that simulate individual fibre structures and a function similar to that proposed by Alsawaf [18]. Discrete models are, however, not preferential due to the computational expense they incur.

Alsawaf [18] proposed a two stage linear function to describe uniaxial deformation of a weave, however instead of linear functions, two exponential functions could be used, one with an initially low stiffness and curvature and a second, which is only implemented when a critical point is reached which has a higher stiffness and curvature. This method may however be difficult to implement, where continuity along the function would need to be enforced and transverse interplay would be difficult to define.

Although time and effort may be spent modeling the fabric and its behavior *ex vivo*, the mechanics of the fabric will change considerably over time *in vivo*. When implanted, cells will seed themselves to the fabric , changing its mechanical behavior. To account for tissue integration and regeneration, the constitutive relationship presented may be extended to incorporate a time dependent model for tissue in-growth. An increase in stiffness with time

can be obtained by increasing C while the orthogonal anisotropy and orientation may be adjusted by varying the a_i, i.e. $C, a_i = f(t)$ such that $C, a_i \rightarrow Limit$ when $t \rightarrow \infty$.

5. Conclusions

The nonlinear anisotropic elastic strain-energy function proved feasible to realistically describe the coupled warp-weft mechanics of a variety of knit fabrics. While the fabric model can provide a tool for the design of implants for e.g. orthopedic and cardiovascular therapies, it does not account, in its current form, for the effects of cell and tissue incorporation. This *in vivo* aspect can be included by extending the model but will require extensive experimental data to obtain a realistic relationship, with variation in material type and fabric construction.

Acknowledgments

This work was funded in part through a research collaboration grant by Medtronic Inc. (Minneapolis, MN, USA) to the University of Cape Town.

Conflict of Interest

The authors confirm that there are no known conflicts of interest associated with this publication.

References

[1] Li, B., Wen, Y., Wu, H., Qian, Q., Wu, Y., Lin, X.. Arthroscopic single-bundle posterior cruciate ligament reconstruction: retrospective review of hamstring tendon graft versus lars artificial ligament. Int Orthop 2009;33:991–996.

[2] Gao, K., Chen, S., Wang, L., Zhang, W., Kang, Y., Dong, Q., et al. Anterior cruciate ligament reconstruction with lars artificial ligament: a multicenter study with 3- to 5-year follow-up. Arthroscopy 2010;26:515–523.

[3] Rotini, R., Fini, M., Giavaresi, G., Marinelli, A., Guerra, E., Antonioli, D., et al. New perspectives in rotator cuff tendon regeneration: review of tissue engineered therapies. Chir Organi Mov 2008;91:87–92.

[4] Burns, J.P., Snyder, S.J.. Biologic patches for management of irreparable rotator cuff tears. Techniques in Shoulder & Elbow Surgery 2009;10:11–21.

[5] Shikinami, Y., Kawabe, Y., Yasukawa, K., Tsuta, K., Kotani, Y., Abumi, K.. A biomimetic artificial intervertebral disc system composed of a cubic three-dimensional fabric. Spine J 2010;10(2):141–152.

[6] Konertz, W.F., Shapland, J.E., Hotz, H., Dushe, S., Braun, J.P., Stantke, K., et al. Passive containment and reverse remodeling by a novel textile cardiac support device. Circulation 2001;104(12 Suppl 1):I270–I275.

[7] Oz, M.C., Konertz, W.F., Raman, J., Kleber, F.X.. Reverse remodeling of the failing ventricle: surgical intervention with the acorn cardiac support device. Congest Heart Fail 2004;10(2):96–104; discussion 105.

[8] Blom, A.S., Pilla, J.J., Arkles, J., Dougherty, L., Ryan, L.P., Gorman, J.H., et al. Ventricular restraint prevents infarct expansion and improves borderzone function after myocardial infarction: a study using magnetic resonance imaging, three-dimensional surface modeling, and myocardial tagging. Ann Thorac Surg 2007;84(6):2004–2010.

[9] Yeoman, M.S., Reddy, B.D., Bowles, H.C., Zilla, P., Bezuidenhout, D., Franz, T.. The use of finite element methods and genetic algorithms in search of an optimal fabric reinforced porous graft system. Ann Biomed Eng 2009;37:2266–2287.

[10] Heim, F., Gupta, B.S.. Textile heart valve prosthesis: The effect of fabric construction parameters on long-term durability. Textile Research Journal 2009;79:1001–1013.

[11] Haas, R., Dietzius, A.. The stretching of the fabric and the deformation of the envelope in nonrigid balloons. In: Annual report 3. National Advisory Committee for Aeronautics; 1917, p. 149–271.

[12] Peirce, F.T.. Geometry of cloth structure. J Text Inst 1937;28:T45.

[13] Kawabata, S., Postle, R., Niwa, M.. Objective specification of fabric quality, mechanical properties and performance. Kyoto: Textile Machinery Society of Japan; 1982.

[14] Hearle, J., Shanahan, W.. An energy method for calculations in fabric mechanics, parts 1 and 2. J Text Inst 1978;69:81–100.

[15] King, M.J., Jearanaisilawong, P., Socrate, S.. A continuum constitutive model for the mechanical behavior of woven fabrics. International Journal of Solids and Structures 2005;42:3867–3896.

[16] Grosberg, P., Kedia, S.. The mechanical properties of woven fabrics. Text Res J 1966;38:71–79.

[17] Hearle, J.W.S., Grosberg, P., Backer, S.. Structural mechanics of fibers, yarns and fabrics. New York: Wiley-Interscience; 1969.

[18] Alsawaf, F.B.. A model for textile tensile curves. Ph.D. thesis; Institute of Science and Technology, University of Manchester; 1985.

[19] Sun, W.. Constitutive modeling of composites incorporating nonlinear and three-dimensional effects. Ph.D. thesis; College of Engineering, Drexel University; 1992.

[20] Mathews, J.. Numerical methods for mathematics, science and engineering. Englewoods, N.J.: Prentice Hall Inc.; 1992.

[21] Hu, J., Newton, A.. Modelling of tensile stress-strain curve of woven fabrics. J of China Textile University 1993;10:49–61.

[22] Bais-Singh, S., Goswami, B.C.. Theoretical determination of the mechanical behaviour of spun-bound nonwovens. J Text Inst 1995;86:271–288.

[23] Bais-Singh, S., Goswami, B.C.. Predicting the biaxial tensile deformation behavior of spunbonded nonwovens. Textile Research Journal 1998;68:219–227.

[24] Collier, J., Collier, B., Toole, G., Sargrand, S.. Drape prediction by means of finite element analysis. J Text Inst 1991;82:96–107.

[25] Kim, J.. Fabric mechanics analysis using large deformation orthotropic shell theory. Ph.D. thesis; Dept of. Mechanical and Aerospace Engineering, North Carolina State University; 1991.

[26] Gan, L., Steven, G., Ly, N.. A finite element analysis of the draping of fabric. In: Proc. 6th int. conference on finite element methods, university of sydney. 1991, p. 402–414.

[27] Yu, W.R., Kang, T.J., Lee, J.K.. Drape properties of woven fabrics. In: Proc. 2nd asian textile conf. 1993, p. 455–459.

[28] Kang, T., Lee, J., Yu, W., Oh, K.. Prediction of woven fabric deformation using finite element method. In: Proc. int. symp. on fiber science and technology, hong kong. 1994, p. 480–481.

[29] Dong, L., Lekakou, C., Bader, M.G.. Solid-mechanics finite element simulations of the draping of fabrics: a sensitivity analysis. Composites Part A: Applied Science and Manufacturing 2000;31:639–652.

[30] Badel, P., Vidal-Salle, E., Boisse, P.. Computational determination of in-plane shear mechanical behaviour of textile composite reinforcements. Computational Materials Science 2007;40:439–448.

[31] Badel, P., Gauthier, S., Vidal-Salle, E., Boisse, P.. Rate constitutive equations for computational

analyses of textile composite reinforcement mechanical behaviour during forming. Composites Part A: Applied Science and Manufacturing 2009;40:997–1007.

[32] Yu, W.R., Harrison, P., Long, A.. Finite element forming simulation for non-crimp fabrics using a non-orthogonal constitutive equation. Composites Part A: Applied Science and Manufacturing 2005;36:1079–1093.

[33] Yu, W.R., Pourboghrat, F., Chung, K., Zampaloni, M., Kang, T.J.. Non-orthogonal constitutive equation for woven fabric reinforced thermoplastic composites. Composites Part A: Applied Science and Manufacturing 2002;33:1095–1105.

[34] Nadler, B., Papadopoulos, P., Steigmann, D.J.. Multiscale constitutive modeling and numerical simulation of fabric material. International Journal of Solids and Structures 2006;43:206–221.

[35] Carvelli, V.. Monofilament technical textiles: An analytical model for the prediction of the mechanical behaviour. Mechanics Research Communications 2009;36:573–580.

[36] Carvelli, V., Corazza, C., Poggi, C.. Mechanical modelling of monofilament technical textiles. Computational Materials Science 2008;42:679–691.

[37] Ramberg, W., Osgood, W.R.. Description of stress-strain curves by three parameters. Technical Note No. 902; National Advisory Committee for Aeronautics; Washington D.C.; 1943.

[38] Chuong, C.J., Fung, Y.C.. Three-dimensional stress distribution in arteries. J Biomech Eng 1983;105:268–274.

[39] Cardiovascular implants - vascular prosthesis [aami vp20]. Arlington, VA: Association for the Advancement of Medical Instrumentation (AAMI); 1994.

[40] Cardiovascular implants - tubular vascular prosthesis [iso 7198]. Geneva: International Organization for Standardization (ISO); 1998.

[41] Gadala, M.S.. Recent advances in numerical modeling of constitutive relations. Finite Element in Analysis and Design 1997;24:171–185.

[42] Hatch, K.L.. Textile science. New York: West Publishing; 1993.

[43] Tong, P., Fung, Y.C.. The stress-strain relationship for the skin. J Biomech 1976;9:649–657.

[44] Faires, J., Burden, R.. Numerical methods. Boston: PWS Publishing; 1993.

Tables

Table 1: Patch test results for uniform and non-uniform multi-element model and single element model for uniaxial tension and simple shear. Ranges are given for the simple shear test. Notations: $S11$, $S22$ Normal stress in 1 and 2 directions; $S12$ Shear stress; $U1$ Displacement in 1 direction.

		Multi Element		**Single**
		Uniform	*Non-uniform*	**Element**
Tensile	$S11$ (Pa)	6.776	6.776	6.776
	$S22$ (Pa)	0.168×10^7	0.168×10^7	0.168×10^7
	$S12$ (Pa)	0.0	0.0	0.0
	$U1$ (mm)	-0.581	-0.581	-0.581
Shear	$S11$ (Pa)	$-0.24\times10^5 \rightarrow 1.75\times10^5$	$-0.23\times10^5 \rightarrow 1.73\times10^5$	0.41×10^5
	$S22$ (Pa)	$-0.188\times10^5 \rightarrow 4.92\times10^5$	$-0.193\times10^5 \rightarrow 4.82\times10^5$	0.59×10^5
	$S12$ (Pa)	$0.072\times10^5 \rightarrow 2.86\times10^5$	$0.097\times10^5 \rightarrow 2.81\times10^5$	0.86×10^5

Table 2: Model coefficients for fabric samples and associated values for the partial objective functions, objective function and fitness function obtained with the genetic algorithm and the number of generations required to obtain the presented solution.

Fabric Sample	1	2	3	4
Coefficients				
C	26444.0	9766.2	12401.0	10299.0
a_1	9.6714	12.77	38.689	81.086
a_2	15.815	15.414	5.2838	35.152
a_3	86.94	12.895	25.122	39.747
a_4	15.742	12.322	19.878	84.289
a_5	-3.8816	2.3294	-9.9038	-22.657
a_6	21.377	-5.3519	0.92224	20.526
a_7	-39.528	-13.246	28.778	43.484
a_8	-5.0215	5.1202	10.485	94.932
a_9	8.5257	-1.9179	12.086	124.26
Fitness Value $f(C, a_i)$	0.99985	0.99962	0.99968	0.99970
Objective Value $\phi(C, a_i)$	0.99985	0.99962	0.99968	0.99970
Partial Objective Values				
$\phi^{\sigma_A^{warp}}$	0.99980	0.99957	0.99998	0.99998
$\phi^{\sigma_A^{weft}}$	0.99993	0.99938	0.99947	0.99974
$\phi^{\varepsilon_A^{warp}}$	0.99972	0.99981	0.99989	0.99987
$\phi^{\varepsilon_A^{weft}}$	0.99938	0.99967	0.99991	0.99980
$\phi^{\varepsilon_T^{warp}}$	0.99991	0.99987	0.99935	0.99934
$\phi^{\varepsilon_T^{weft}}$	0.99981	0.99993	0.99979	0.99935
Generation	47	42	39	45

Figure Captions

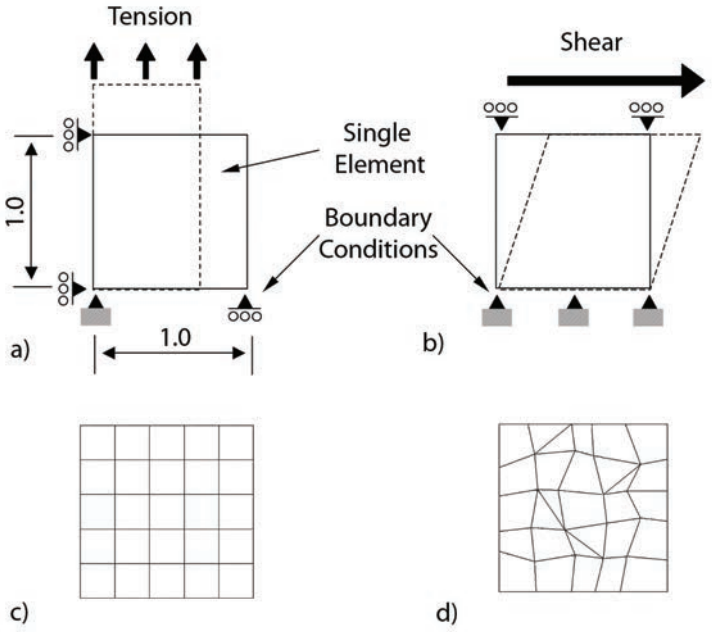

Figure 1: Patch test models: Single element models for a) uniaxial tension and b) simple shear; Multi element models with c) uniform and d) non-uniform mesh.

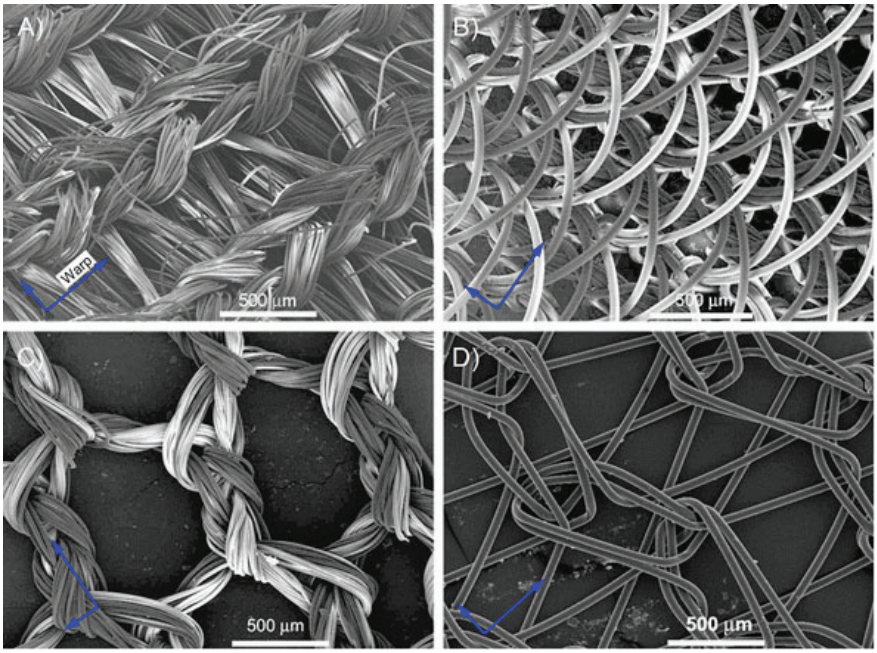

Figure 2: Scanning electron micrographs (50x) of fabrics tested; (A) sample 1: basic warp knit, (B) sample 2: warp knit with Lycra® support, (C) sample 3: coarse warp knit and (B) sample 4: monofilament warp knit. (Arrows indicate warp/weft directions.)

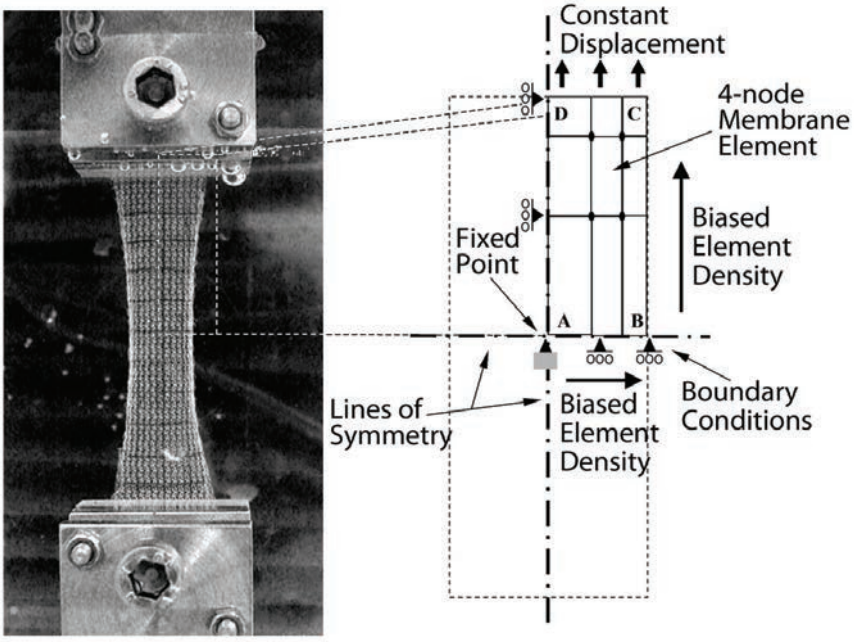

Figure 3: a) Photograph of fabric sample and customized clamps during uniaxial tensile test and b) Finite element model for uniaxial tensile test utilizing symmetry.

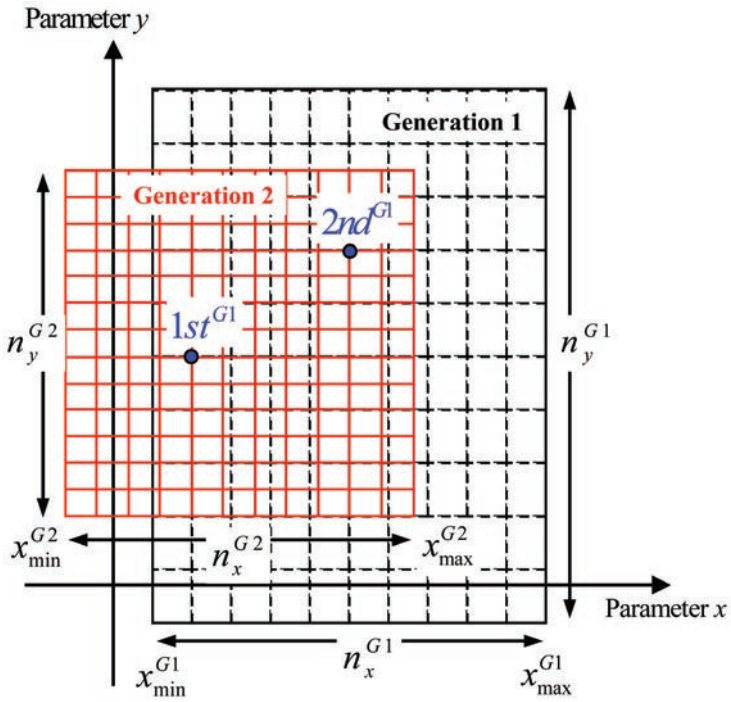

Figure 4: Schematic illustrating the reduction of a two-dimensional parameter search space from ($x^{G1}_{\max}-x^{G1}_{\min}$) to ($x^{G2}_{\max}-x^{G2}_{\min}$), biased 3 : 2 between the first and second ranked solutions of generation 1 ($1st^{G1}$, $2nd^{G1}$) and the resolution of the search increased from n^{G1}_x to n^{G2}_x for parameter x and n^{G1}_y to n^{G2}_y for parameter y.

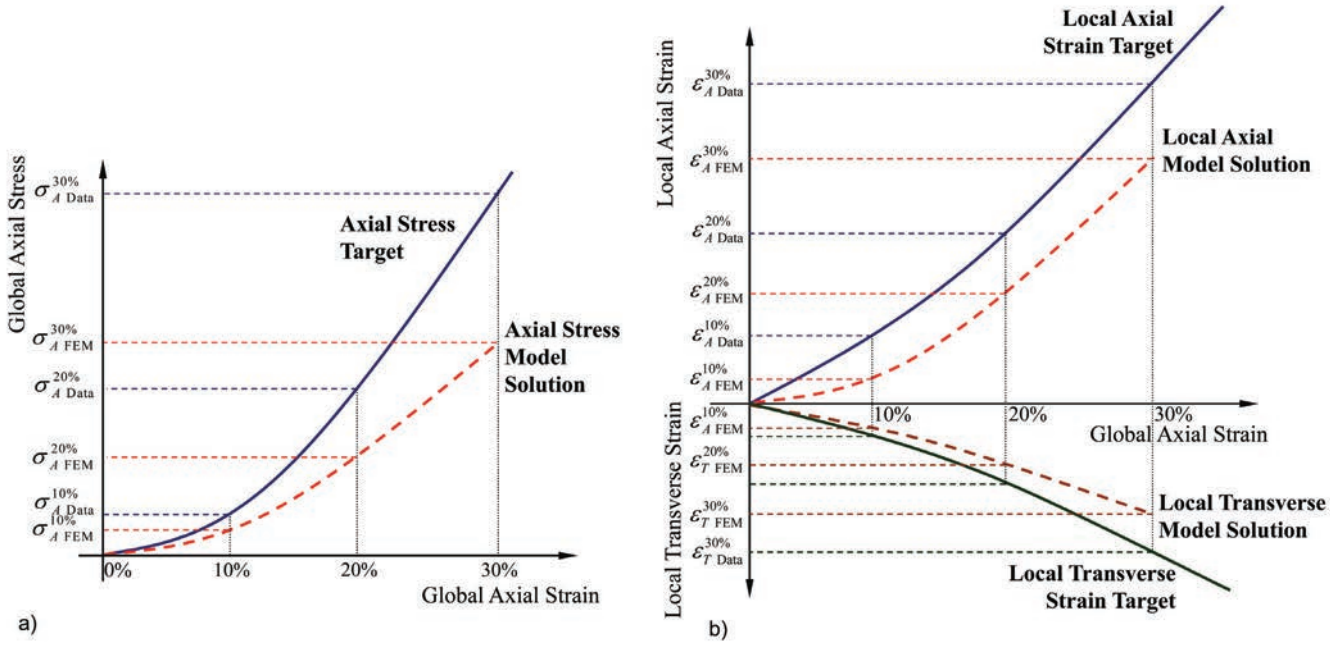

Figure 5: Uniaxial tensile numerical solution vs. target solution.

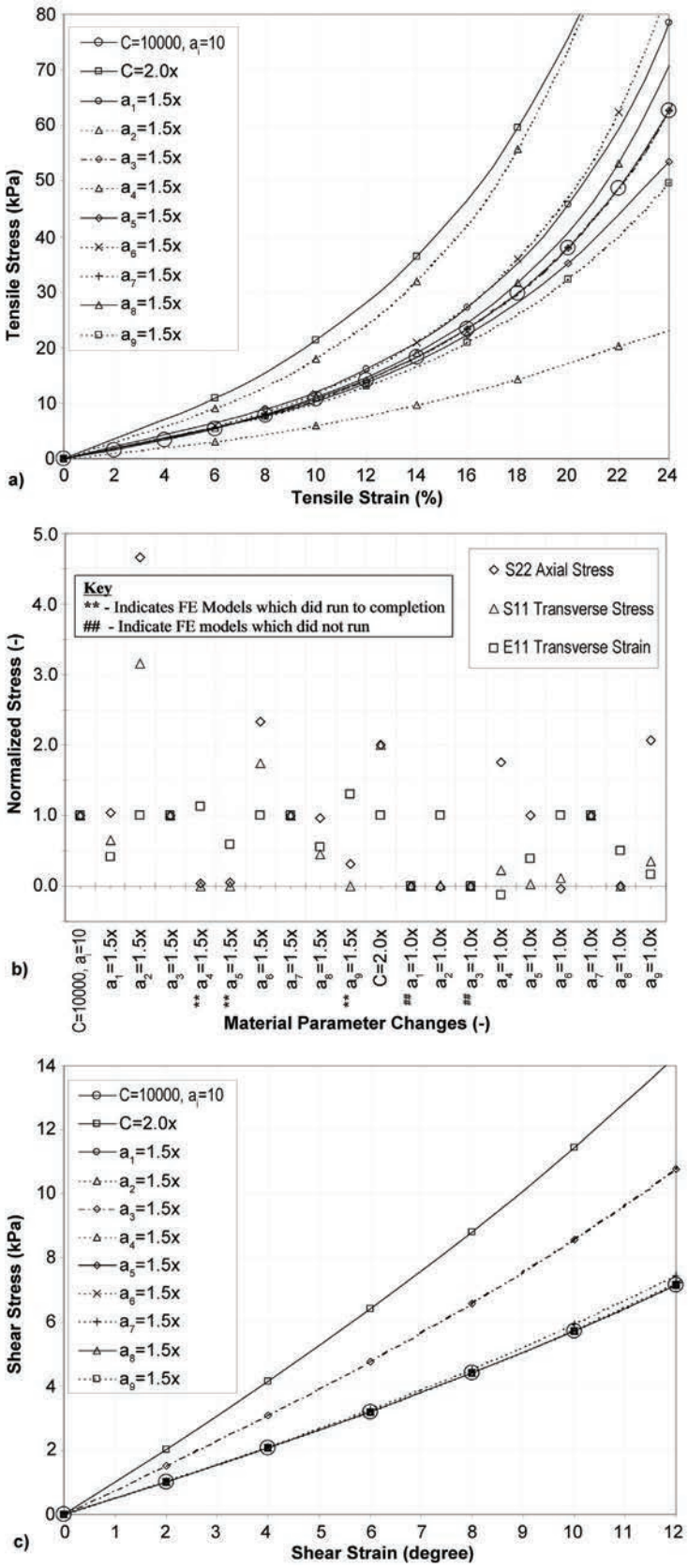

Figure 6: Effects of fabric material coefficients C and a_i: a) Stress-strain curves and b) normalized stress and transverse strain for uniaxial tension; c) Shear stress - shear angle curves.

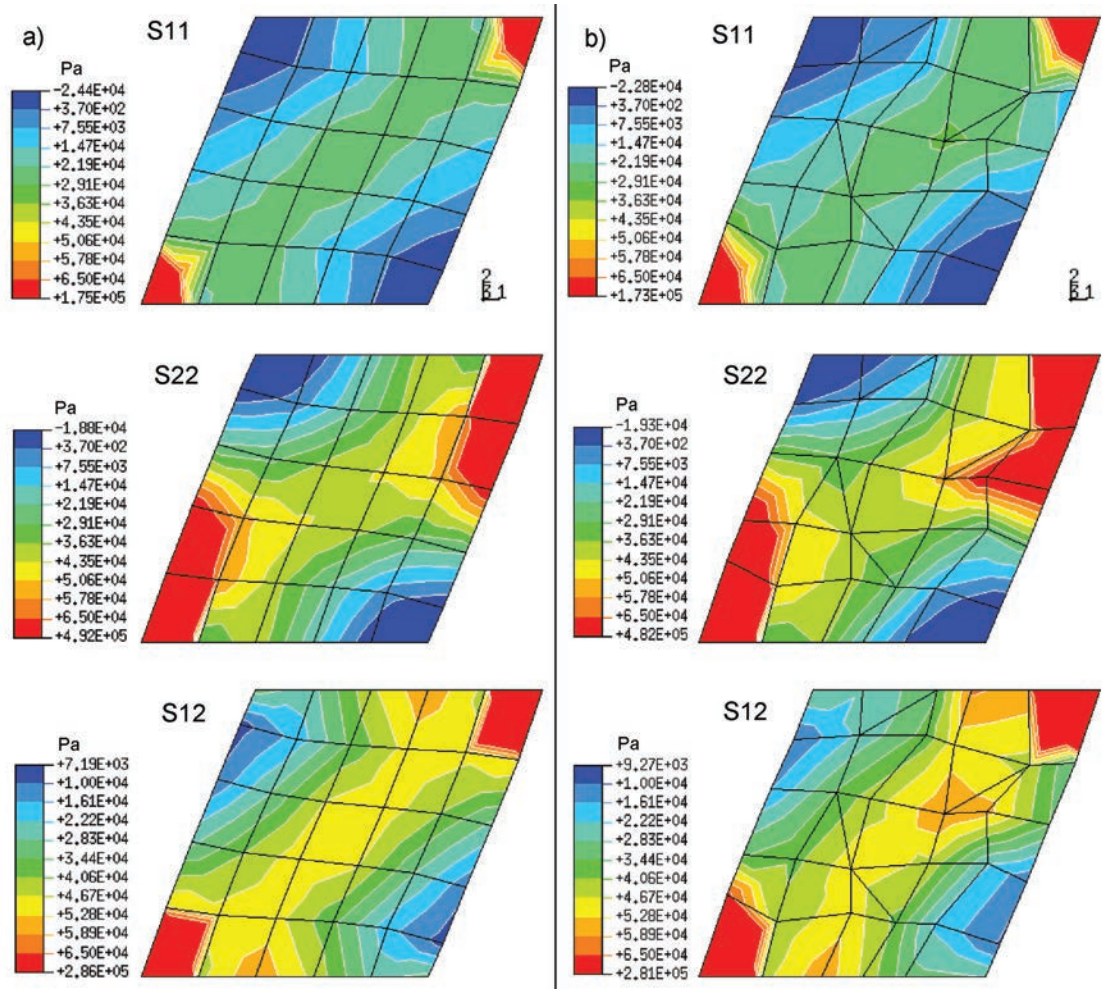

Figure 7: Contour plots of normal stresses ($S11$, $S22$) and shear stress ($S12$) for a) uniform and b) non-uniform multi-element shear patch test models. (A color version is available as online supplementary material.)

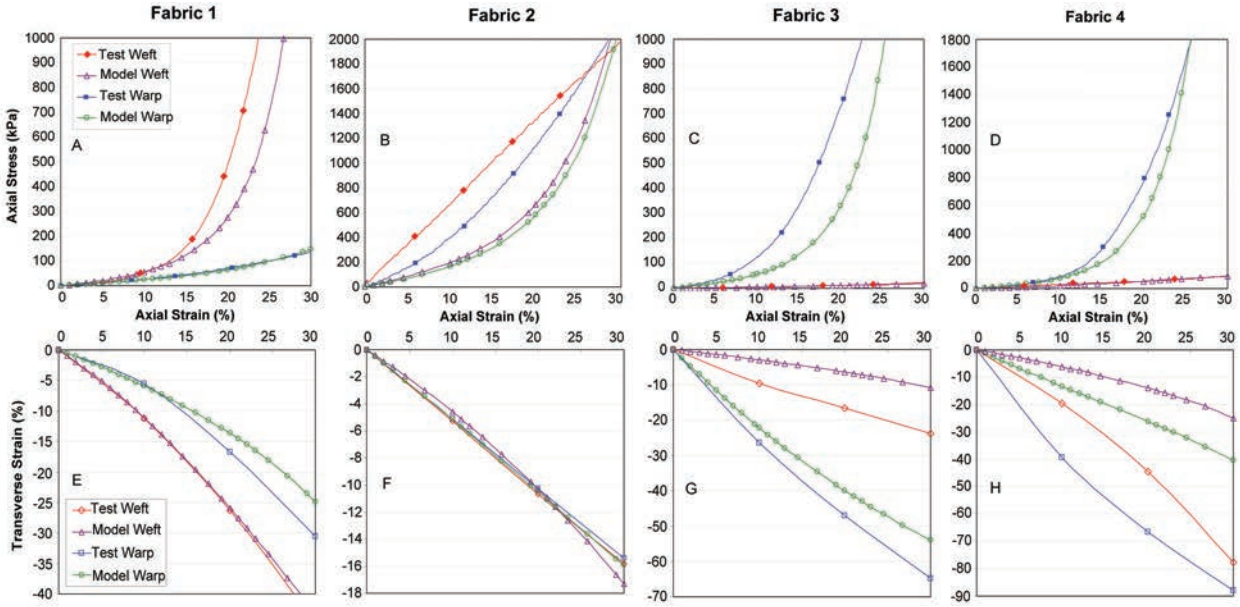

Figure 8: Nominal stress and engineering strain data of physical tensile tests and model predictions for the warp and weft direction of fabrics 1 to 4: A-D) Uniaxial tensile stress versus axial strain, E-H) Transverse strain versus axial strain.